Electronic Structure of Transition Metal Oxide Nanostructures

J. M. Sanz[1], G.T.Tyuliev[2], C.Morant[1], L.Soriano[1], J.P.Espinós[3], A. Fernández[3] and A. R. González-Elipe[3]

[1]*Dpt. Física Aplicada C-XII. Universidad Autónoma de Madrid. Cantoblanco. E-28049 Madrid. Spain.*
[2]*Institute of General and Inorganic Chemistry. Bulgarian Academy of Sciences. 1113-Sofia. Bulgaria.*
[3]*Instituto Ciencia de Materiales de Sevilla, CSIC-Universidad de Sevilla. Avda. Américo Vespucio, s/n. Isla de la Cartuja. 41092 Sevilla. Spain.ABCDEFGHIJKLMNOPQRSTUVWXYZ*

(Received: Jan. 31, 1997 Accepted: Feb. 20, 1997)

Abstract

We report on the use of large area electron spectroscopies like X-ray photoemission, resonant photoemission and X-ray absorption spectroscopy, to probe the electronic structure of nanoparticles and ultrathin films of transition metal oxides. Highly defective NiO nanoparticles (2-5 nm) have been studied using X-ray and electron spectroscopies. The Ni2p XAS spectrum shows convincingly that these particles do not involve Ni as previously thought. The high sensitivity of the Ni2p XPS core level lineshape to the local coordination of the nickel atoms (i.e. to defects, nearest and next nearest neighbours) is demonstrated studying the growth of ultrathin NiO films on MgO(100). The use of resonant photoemission to identify the Ti3d derived valence band states in the valence band of ultrathin TiO_2 films grown on SiO_2 is also shown.

1. Introduction.

The preparation and characterization of low dimensional and nano-structures of transition metal oxides (TMO) are topics of great interest in several branches of basic and applied research, as they exhibit interesting physical and chemical properties, which differ significantly from those of the bulk material. In general, these nanostructures require an extensive chemical, crystallographic thermodynamic, mechanical and electronic characterization, that unfortunately not always is possible. In fact, the electronic structure of TMO's appears to be much less understood than those of metals and semiconductors[1-3]. Electron spectroscopies give the most detailed and relevant information about the electronic structure, but in many cases, problems of surface charging make extremely difficult and sometimes impossible the use of such techniques. Over the last years a lot of supported small particles (mostly metals on oxides, more scarcely oxides on oxides) have been studied by XPS, UPS and AES, so that the general experimental results appear well established; i.e. energy shifts in photoemission, Auger and X-ray absorption edges as well as changes in X-ray edge intensities, photoemission valence band intensities and splitting and photoemission and Auger line widths. The observed effects are usually explained as a size dependence of the initial state electronic structure, or due to variations in the final state relaxation processes [4]. However, many times, those effects appear masked by strong interactions with the substrate, the lack of long range order, a high density of defects or many other subtle effects [4-6]. All of these complexities, in addition to the fact that good theoretical calculations of even the ground state electronic configuration for most metal oxides is lacking, make it difficult the interpretation of the experimental data and leads to long standing controversies.

Nevertheless, experimentally, much information can be expected to be given by surface sensitive techniques such as x-ray and electron spectroscopies. In this work we report on the use of large area spectroscopies, i.e. Photoelectron Spectroscopies (XPS and PES), Resonant Photoelectron Spectroscopy (RPES) and X-ray Absorption Spectroscopy (XAS.), to obtain significant information on the electronic structure of TMO nanostructures.

2. Electronic Structure of TMO Nanostructures.

2.1 NiO nanoparticles

NiO nanoparticles (2-5 nm), prepared according to the method described by Gravelle and Teichner [7], are well known to exhibit interesting catalytic, electric and magnetic properties, whose origin has been associated with their size and a high density of defects. In fact, defects are considered a key factor controlling the catalytic properties of this material, but their characterization and their influence on the electronic structure is still controversial [1,10-14].

Fig.1 shows the respective $Ni2p_{3/2}$ (Fig.1a) and

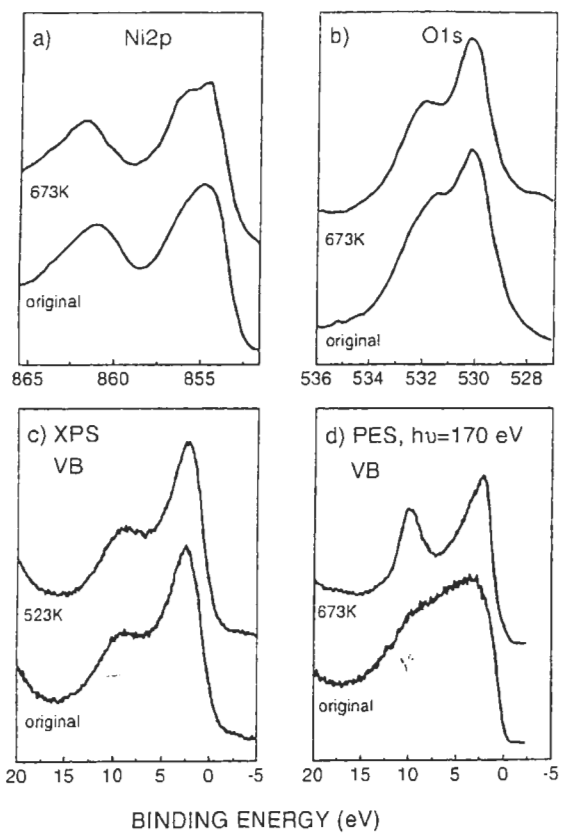

Fig. 1 (a) $Ni2p_{3/2}$, (b) O1s, (c) XPS valence band and (d) PES valence band spectra of NiO nanoparticles as introduced and after heating as labelled.

O1s (Fig.1b) XP spectra for a pellet of these nanoparticles as received and after heating at 673 K, as labelled. An important feature at the O1s and Ni2p spectra is the appearance of satellites 1.7 eV above the binding energy of the respective main lines, whose intensities decrease significantly after heating. In previous XPS studies these features have been associated

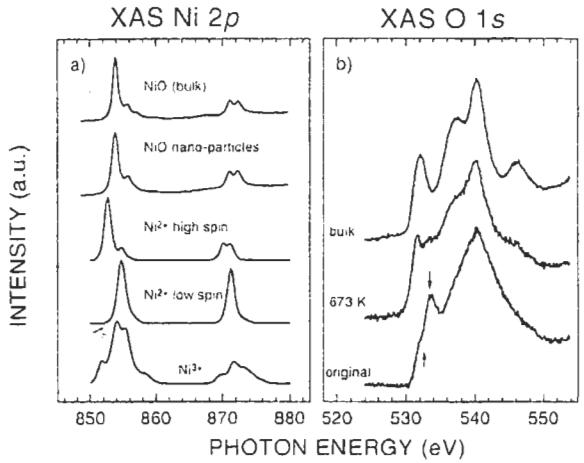

Fig. 2 (a) Ni 2p XAS spectra of stoichiometric NiO and the nanoparticles of NiO as labelled. Multiplets calculations for Ni^{2+} with high spin symmetry, Ni^{2+} with low spin symmetry and for Ni^{3+} are also included. (b) O1s XAS spectra of stoichiometric NiO, and of the NiO nanoparticles as introduced and after heating at 673K, as labeled.

with the presence of Ni^{3+} species at defective sites [8-13]. However, the Ni2p X-ray absorption spectrum shows convincingly that these particles do not involve Ni^{3+} as thought for decades [8-13]. The Ni2p X-ray absorption spectra of a reference NiO sample and of the defective nanoparticles have been depicted in Fig.2a, as labelled.

The spectra correspond to transitions $2p^63d^8 \rightarrow 2p^53d^9$ and are clearly dominated by multiplet effects. The spin-orbit interactions lead to two groups of multiplets around 854 and 872 eV. The spectrum for bulk NiO agrees well with previous data and has been discused in detail in Ref. 14. The spectrum for the defective nanoparticles shows only minor changes with respect to that for bulk NiO. The onset of the Ni4s states around 866eV can not be distinguished and the relative intensity of the peaks in the $2p_{1/2}$ edge has changed. These effects can be explained in terms of disorder and a small decrease in the crystal field splitting with respect to bulk NiO [14,15]. Fig.2a also shows atomic multiplet calculations of the Ni2p absorption edge [15] for NiO in different configurations (i.e high and low spin Ni^{2+} and Ni^{3+} for a crystal field parameter of 1.8 eV). The high spin Ni^{2+} spectrum shows the best agreement with both the spectra obtained for bulk and defective nanoparticles of NiO. Although a shift of 0.6 eV is cleanly observed between the calculated and the experimental spectra. We have kept the

calculated energy scale. Therefore, this experimental observation determines unambiguously that the formal valency of nickel in the highly defective NiO nanoparticles is Ni^{2+} in clear contradiction with the common assumption that the doubly peaked Ni2p main line observed with XPS was due to the presence of Ni^{3+} [16].

Fig.2b shows the O1s X-ray absorption spectra of a bulk NiO sample as compared with those of the NiO nanoparticles as introduced and after heating at 673K. The spectra correspond to transitions to unoccupied states with Op character, but with significant metal character due to metal-ligand hybridization. The peak at the edge in the spectrum of bulk NiO corresponds to Ni3d-O2p hybridization (i.e. e_g subband). The bumps around 537 and 540.5 eV are related to Ni4p bands and the weak feature at 546.5 to Ni4s states. When compared with it, the O1s spectra of the nanoparticles shows a clear split of the edge to lead a second peak at 533.7 eV (i.e. 1.7 eV above the O1s edge of bulk NiO). This second peak is even more intense than the low energy edge for the original nanoparticles, but decreases rapidly when the sample is heated above 673K to approach the shape of bulk NiO. This, clearly indicates the presence of adsorbed oxygen species in the defective sites, in good agreement with the two oxygen species observed by XPS (cf. Fig1b).The nanoparticles also show a significant broadening of the Ni4p bands, so that the Ni4s band can not be distinguished. This is in agreement with the above observation in the Ni2p spectrum. Annealing causes the desorption of adsorbed species and some rearrangement of the atoms until all the bonds saturate as in bulk NiO and leads to a spectrum that is in general agreement with that of bulk NiO [16]. For completeness we have included in Fig.1c and d the corresponding valence band photoemission spectra measured with photons of 1253.6 eV (XPS) and of 170 eV (PES). The differences in the Ni3d and O2p cross sections at those photon energies makes the spectrum measured at 170 eV much more sensitive to the O-derived adsorbed species Annealing causes the desorption of adsorbates so that after heating above 523K the spectrum seems rather similar to that of bulk NiO, except for the high intensity of the satellite around 10 eV observed in PES. These spectra should also reflect the distortion of the t_{2g} levels due to the high density of defects and the oxygen species chemisorbed on the surface. However the spectra are strongly affected by the adsorbed species and difficult its observation [16].

In summary, the electronic structure of highly defective NiO nanoparticles (2-5 nm) has been studied by photoemission and XAS. The results indicate that defects in these nanoparticles are probably associated to unsaturated bonds, which affect the local coordination and symmetry of the nickel ions, and act as active sites for chemisorption. All that causes important changes in the XPS core lines spectra as well as in the O1s and Ni2p XAS spectra. In any case it is concluded that Ni^{3+} species are not present at the surface of these defective nanoparticles [16]

2.2 Ultrathin films of NiO on MgO(100).

As mentioned above, core level XPS at the Ni 2p edge, has been used for decades to study the surface of NiO [10-13]. In fact, it has been extensively used in connection with the identification of defect structures. The important feature here was the satellite peak at around 1.7 eV higher binding energy than the main Ni2p line in both edges (i.e $2p_{3/2}$ and $2p_{1/2}$). Although the satellite is known for decades its origin is still controversial [13, 17-23]. An extended explanation has been recently proposed by Van Veenendaal and Sawatzkty [22] in terms of a screening mechanism that requires at least two sites and is referred to as nonlocal screening. These authors conclude that the satellite structure is intrinsic for NiO, but the detailed line shape is strongly influenced not only by nearest neighbors but also next-nearest-neighbors configurations and therefore

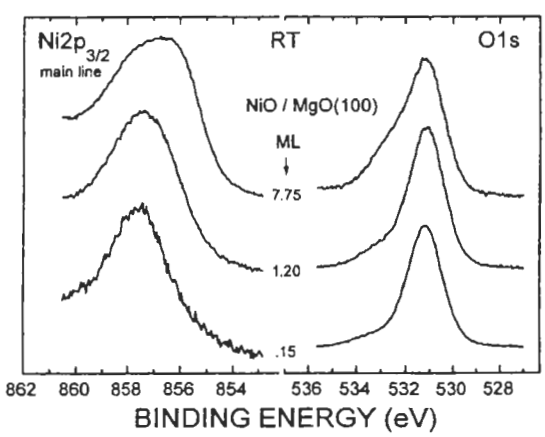

Fig. 3 Ni $2p_{3/2}$ and O1s XPS spectra for NiO films of different thickness, grown on MgO(100) at room temperature.

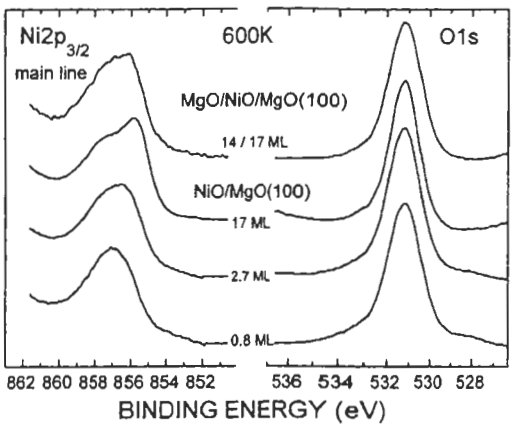

Fig. 4 Ni $2p_{3/2}$ and O1s XPS spectra for NiO films of different thickness, grown on MgO(100) at 600K. The spectra corresponding to the growth of 14ML of MgO on top of 17 ML of NiO are also included.

it is strongly dependent on the details of the structure. This fact appeared to be interesting for the characterization of supported nanostructures, where the interaction with the substrate is significant.

In the following we present an study of the growth of NiO on MgO(100) in terms of the Ni2p XPS core lineshape. The main aim was to follow the changes in the Ni2p spectrum when the initial Mg^{2+} neighbours at the interface NiO/MgO, are replaced by Ni^{2+} as the film thickens. We mainly focus on the observation of non-local screening effects in the Ni 2p XPS line and their dependence on the grown structure. The following results demonstrate the sensitivity of the core level line shape to the nearest and next nearest neighbours coordination [21-23]. NiO was deposited on MgO(100) by evaporation of nickel in an oxygen atmosphere. The experimental details can be found in Ref. 21.

The layer thickness dependence of the $Ni2p_{3/2}$ XPS spectra of epitaxially grown NiO on MgO(100) substrate at room temperature and at 600K, is shown in Figs.3 and 4 respectively. Both figures include the accompanying O1s spectra For coverages below 1 ML the $Ni2p_{3/2}$ main line consists in just one broad (FWHM 2.5-2.8 eV) line centered at 857.6 eV. At higher coverages an extra feature appears on the low binding energy side, and its position for bulk NiO is 855.8 eV. For clean MgO the O1s signal is a single peak at 531.2 eV that we assign to O^{2-} lattice oxygen. Increasing the NiO film thickness at room temperature, the main O^{2-} peak preseves its position but a high binding energy shoulder at 532.8 eV appears. This is called "excess oxygen" in the literature [10-12] and is usually associated with adsorbed species at defect sites, which are very active for chemisorption. The films grown at 600K (cf. Fig.4) show only one symmetric O1s peak, and the Ni2p peak shows a higher main line to satellite intensities ratio. All that indicates that the growth at high temperature yields NiO films of a higher quality and fewer defects, because defects would lead to the adsorption of oxygen species which would give rise to more intense higher binding energy shoulders in both the O1s and $Ni2p_{3/2}$. Similar results have been published recently by Alders and Sawatzky [23], except that hey do not show spectra for coverages bellow 1ML.

Taking into account that NiO grows on MgO (100) in a layer by layer mode [24,25]. The Ni2p photoemission spectra at coverages below 1ML can be considered as due to Ni^{2+} ions coordinated with oxygen anions and having Mg^{2+} ions as next nearest neighbors (i.e. the MgO substrate). For these coverages only one broad peak in the $Ni2p_{3/2}$ main line is observed at 857.6eV. Similar spectra have been observed for Ni^{2+} ions well dispersed in TiO_2 [26]. At higher coverages a second feature on the low binding energy side appears and grows with thickness, so that the relative intensity with respect to the original feature depends on the thickness of the layer. Obviously it seems to be due to the presence of Ni^{2+} ions as next nearest neighbors. Therefore, if as established by van Veenendaal and Sawatzky [22] the doublet is inherent to the formation of NiO, this compound seems not to be formed until more than a complete layer has been grown. In fact, only for coverages above 3ML, the low binding energy peak is more intense than the satellite [21], suggesting that the influence of the substrate is significant until this thickness is reached. It is interesting to mention the difference in FWHM of both features, whereas the low binding energy component is sharp (i.e FWHM=1eV) the FWHM of the satellite is about 2.5 eV. All that sesitivity to the local coordination of the Ni^{2+} ions can be pointed out by the analysis of ultrathin NiO buried layers (i.e. MgO/NiO/MgO). Fig.4 includes a spectrum due to 14ML MgO grown on top of 17 ML of NiO. Comparing the lineshape of the $Ni2p_{3/2}$ spectrum for the 17 ML of NiO before and after MgO deposition we can observe a

rather subtle change. The figure clearly indicates a transfer of intensity from the main line to the satellite which is in the inverse direction as that observed during the growth of NiO on MgO(100). Again, those effects can be explained as due to changes in the coordination of the Ni cations and the presence of Mg^{2+} ions. Therefore, all those changes seem to be the result of a complex interplay between local and non-local screening mechanisms as proposed by van Veenendaal and Sawatzky [22]. In fact, they seem to be very sensitive to sample preparation, defects and surface crystallinity [21-23].

2.3 Resonant Photemission of ultrathin TiO_2 films on SiO_2

Resonant Photoemission Spectroscopy (RPES) is a well established technique to study the electronic structure of TM oxides, in particular, to examine the hybridization between the metal and the surrounding oxygen [1]. In the case of TiO_2, the photoemission of Ti3d derived states is significantly enhanced when the photon energy is swept through the Ti3p excitation threshold. The core electron is excited into a highly localized state and its decay via an autoionization process leads to excitation of a d-electron from the occupied part of the valence band. In addition direct photoemission from the occupied VB yields a photoelectron of the same kinetic energy. Since both processes link the same initial and final states, they interfere and give rise to a resonantly enhaced Ti3d photoelectron intensity. By this manner the Ti3d contribution to the VB can be pointed out.
In the present study we have used RPES to characterize the electronic structure of a very thin layer (i.e. 1 equivalent monolayer) of TiO_2 on SiO_2. Synchrotron radiation allows us to measure the resonant photoemission effects of the valence band of TiO_2 associated with Ti3d derived states.
Valence band spectra were taken in the angle resolved mode for different photon energies in the 30-70 eV energy range at a grazing angle (i.e.18° to the surface normal) to enhance the surface sensitivity. Representative spectra for a very thin (~1 ML) TiO_2 are shown in Fig.5. The plot corresponds to the isolated TiO_2 contribution to the total VB, obtained after subtraction of the SiO_2 signal from the substrate and a Shirley background. The spectra are dominated by a broad band, primarily due to O2p derived states.

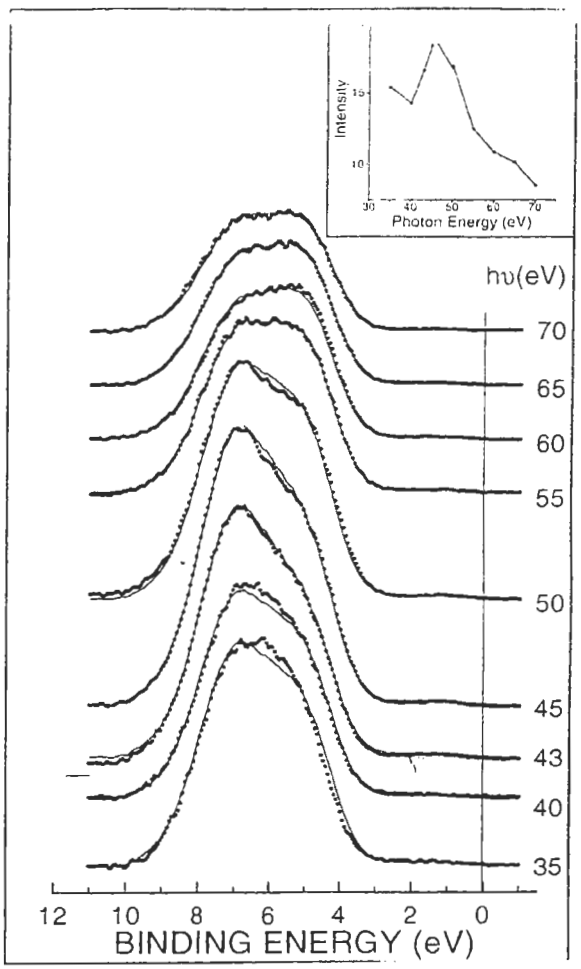

Fig. 5 Experimental valence band photoemission spectra at different photon energies of a very thin TiO_2 film (1ML thick) deposited on SiO_2 (dots) and their fitting (lines) in terms of two components by FA (cf. Fig.6). The inset shows the intensity of the valence band as a function of the photon energy.

The effects associated with changing the photon energy, i.e. the resonant process are clearly observable at a photon energy of ~47 eV. The inset of the figure shows the dependence on the photon energy of the total intensity of the valence band. The resonance profile shows a behavior similar to that for bulk TiO_2 [27]. In particular, the profile is characterized by a maximum around $h\nu \approx 47$ eV and an onset at $h\nu \approx 40$eV. This effect correspond to an enhancement of the Ti3d photoelectron yield when the photon energy is swept over the Ti3p threshold [28].
Since RPES delivers only the enhancement of the Ti3d derived emission, difference spectra measured at the resonance maximum and off resonance should reflect the Ti contribution to the O2p valence band. The 47/50 difference

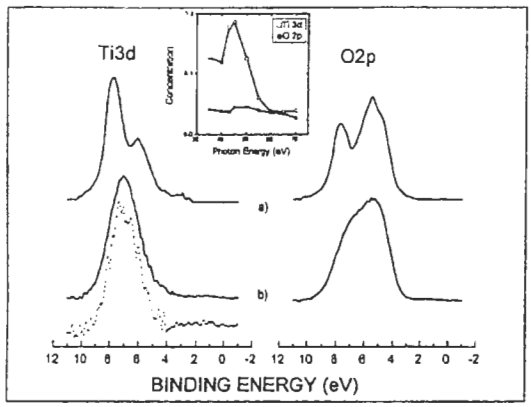

Fig. 6 (a) Calculated Ti3d- and O2p- partial density of states of TiO_2 (rutile) [28] used as target basis in Factor Analysis. (b) Recalculated basis as given by FA (solid lines). Ti3d contribution to the valence band as derived from the resonance at $h\nu \approx 47$ eV (dots). The inset shows the photon energy dependence of the two principal components (Ti3d and O2p) determined by FA.

spectrum; i.e. spectrum at $h\nu=50$ eV (off resonance) subtracted from that at $h\nu=47$ eV (on resonance), is shown as a dotted curve in Fig 6. For comparison we have included the calculated Ti3d partial density of states as given by Munnix and Schmeits [28] for rutile (Fig. 6a). Obviously we can not expect a perfect TiO_2 rutile structure in such a film grown on amorphous SiO_2. However, the general behavior is similar to that expected for bulk TiO_2. Although the experimental data do not resolve the features given by the theory, the agreement existing between the 47/50 difference spectrum and the calculated Ti3d PDOS can be considered as good and confirms the interpretation of the observed resonance at $h\nu=47$ eV as due to Ti3d states. Furthermore, the difference spectrum identifies unambiguously a significant cationic contribution to the valence band of TiO_2, mainly located at the high binding energy side (i.e. the bonding part) of the valence band. In order to gain a more quantitative insight into the resonance and to separate the behavior of both the Ti3d and O2p contributions to the valence band, we have performed Factor Analysis (FA) of the series of spectra of Fig.5 [29]

Factor Analysis is a standard procedure of data handling in analytical chemistry which has been extensively used in AES and core level XPS and other spectroscopies. For details see references 30 and 31. FA enables the determination of the number of relevant components and their concentrations, that can be linearly combined to reproduce a sequence of experimental spectra. Principal Component Analysis of the spectra indicates that two is the minimum number of canonical basis which can reproduce the whole series of spectra. Obviously, these should correspond to the O2p and Ti3d states. Target Testing in terms of the O2p- and Ti3d- partial density of states obtained from theoretical band structure calculations lead to recalculated basis and the respective concentrations which reproduce the experimental sequence of spectra as a linear combination of the basis. The calculated spectra are given as full lines in Fig.5. The recalculated basis given by FA have also been depicted in Fig.6b, to be compared with calculated Ti3d-PDOS and O2p-PDOS and the Ti3d-contribution determined by subtraction of experimental spectra (i.e. 47/50). The agreement is rather good, if we consider the obvious differences between the structure of the grown film and that of rutile. The concentrations corresponding to the respective basis have been depicted in the inset of Fig.6 as a function of the photon energy. These concentrations are, in fact, proportional to the respective experimental photoemission cross sections. After decomposition in d and p-contributions, the behavior of the d- part shows a broad Fano-like resonance, with a maximum at $h\nu \sim 47$ eV in agreement with the Ti3p $\rightarrow$3d* excitation, and a minimum at $h\nu \approx 40$ eV also in good agreement with the Ti3p binding energy. The behavior of the p-cross section is rather flat as it corresponds to the small energy range, that has been swept. The general behavior is rather similar to that observed for bulk TiO_2 [27]. In fact, a more detailed and comparative study with respect to thicker films is necessary in order to observe effects due to the interaction with the substrate. However, it appears that the charge at the Ti site does not change significantly due to interactions with the SiO_2 substrate; i.e. initial state effects seem to be rather small.

3. Conclusions

The electronic structure of TMO nanostructures can be probed by large area spectroscopies like photoemission, resonant photoemission or X-ray absorption spectroscopy. We have presented some selected examples where X-ray and electron spectroscopies have been used to elucidate different aspects of the electronic

structure of several TMO nanostructures. RPES has been used to identify the Ti3d/O2p hybridization in the valence band of an ultrathin TiO_2 film grown on SiO_2. Nanoparticles of NiO and NiO/MgO have been studied by PES, core level XPS and XAS, showing that important information can be obtained by a complementary use of these techniques. We have shown that Ni^{3+} is not present in highly defective NiO nanoparticles, and that the lineshape of the Ni2p XPS line in NiO is very sensitive to the local structure, i.e. defects, nearest and next nearest neighbours, as well as to the thickness of the film or the size of the structure.

Acknowledgments
We thank the financial support of the DGICYT of Spain (PB93-0240) and of the HCM program of the UE (ERBCHRX-CT-930358 and CHGE-CT93-0027 at Bessy).

References

1. V.E. Henrich and P.A. Cox, *The surface science of metal oxides*, Cambridge University Press, Cambridge (1994).
2. V.E. Henrich, Progress in Surface Science 50 (1995) 77.
3. W. Hirschwald in *Surface and near surface chemistry of oxide materials*, ed. J. Nowotny and L-C Dufour, Elsevier, Amsterdam (1988).
4. V. Jiménez, A. Fernández, J.P. Espinós, A.R. González-Elipe, Surf. Sci 350 (1996) 123.
   V.M. Jiménez, J.P. Espinós and A.R. González-Elipe, Surf. Sci 366(1996) 545(1996).
5. Z. Zang and V.E. Henrich, Surf. Sci. 277 (1992) 263.
6. A. Catana, J.P. Locquet, S.M. Paik and I.K. Scullerm, Phys. Rev. B 46 (1992) 15477.
7. P.C. Gravelle and S.J. Teichner, Adv. Catal. 20 (1969) 167.
8. G. Pacchioni, G. Cogliandro and P.S. Bagus, Surf. Sci. 255 (1991) 344.
9. J.M. Blaisdell and A.B. Kunz, Phys. Rev. B 29 (1984) 988.
10. M. Tomellini, J. Chem. Soc., Faraday Trans. I 84 (1988) 3501.
11. M.W. Roberts and R.St.C. Smart, J. Chem. Soc., Farad. Trans. I 80 (1984) 2957.
12. A.R. González-Elipe, J.P. Holgado, R. Alvarez and G. Munuera, J. Phys. Chem. 96 (1992) 3080
13. St. Uhlenbrock, Chr. Scharfschwerdt, M. Neumann, G. Illing and H.J. Freund, J. Phys. Condens. Matter 4 (1992) 7973.
14. G. van der Laan, J. Zaanen, G.A. Sawatzky, R. Karnatak and J.M. Esteva, Phys. Rev. B 33 (1986) 4253.
    J. van Elp, B.G. Searle, G.A. Sawatzky and M. Sacchi, Solid State Commun. 80 (1991) 67
15. F.M.F. de Groot, J.C. Fuggle, B.T. Thole and G.A. Sawatzky, Phys. Rev. B 42 (1990) 5459.
16. L. Soriano, M. Abbate, J. Vogel, J.C. Fuggle, A. Fernández, A.R. González-Elipe, M. Sacchi and J.M. Sanz, Chem. Phys. Lett. 208 (1993) 460.
    L. Soriano, M. Abbate, A. Fernández, A.R. González-Elipe, F. Sirotti, G Rossi, and J.M. Sanz, (to be published)
17. M. Oku, H. Tokuda and H. Hirokawa, J. Electron Spectrosc. Rel. Phenom 53 (1991) 201.
18. K.S. Kim and R.E. Davis, J. Electron Spectrosc. Rel. Phenom. 1 (1972) 251.
19. M. Oku and K. Hirokawa, J. Electron Spectrosc. Rel. Phenom. 10 (1977) 103.
20. S. Hüfner and G. Wertheim, Phys. Rev. B 8 (1973) 4857.
21. J.M. Sanz and G.T. Tyuliev, Surf. Sci. 367 (1996) 196.
22. M.A. Veenendaal and G.A. Sawatzky, Phys. Rev. Lett. 70 (1993) 2459.
23. D. Alders, F.C. Voogt, T. Hibma and G.A. Sawatzky, Phys. Rev. B 54 (1996) 7716.
24. D.M. Lind, S.D. Berry, G. Chern, H. Mathias and L.R. Testardi, Phys Rev. B 45 (1992) 1838.
25. S.D. Peacor and T. Himba, Surf. Sci. 301 (1994) 11.
26. J.P. Espinós, A.R. González-Elipe and G. Munuera, Solid State Ionics 63-65 (1993) 748.
27. Z. Zhang, S.P. Jeng and V.E. Henrich, Phys Rev B 43 (1991) 12004
28. S. Munnix and M. Schmeits, Phys. Rev. B 30 (1984) 2202.
29. E.R. Malinowsky and D.G. Howery, *Factor Analysis in Chemistry*, Wiley, New York (1980).
30. S.W. Gaarestrom, J. Vac. Sci. Technol. 20 (1982) 458 and Appl. Surf. Sci. 26 (1986) 561.
31. J. Steffen and S. Hofmann, Surf. Interface Anal. 11 (1988) 617.
    S. Hofmann and J. Steffen, Surf. Interface Anal. 14 (1989) 59.